

A short-lived geothermal mud pot near Niland, Imperial County, California

Paul M. Adams¹ and David K. Lynch²

¹126 South Helberta Ave. #2, Redondo Beach, CA, paul.m.adams@aero.org

²dave@caltech.edu

ABSTRACT—A hot (53°C), ~1.2 m diameter mud pot/spring appeared in a farmer's field near Niland, CA in May 2018. It was located in the Wister Fault zone and changed rapidly week by week. By November 22, 2018 it had ceased flowing and had been partially dissected by an irrigation ditch that provided a cross sectional view of the dry vent. The depression and an upper apron surrounding it were covered with a thin layer of rippled white aragonite. An interesting aspect of the vent was the presence of minute shiny black ooids, which formed a subsurface layer and a thin coating on the aragonite apron. The ooids consisted of nuclei of sand grains, with a thin overcoat of aragonite. The black color is attributed to the presence of thin discontinuous layers of iron sulfide in the overcoat. The formation of the ooids seems to be analogous to the formation of cave pearls, whereby calcite-aragonite is precipitated around a nucleus as a result of continuously agitated water saturated in calcium carbonate.

Introduction

The Salton Trough is a topographic low in southern California and northern Baja and Sonora Mexico that represents the transition between the San Andreas Fault system and rifting centers in the Gulf of California.¹ The area is seismically active and has a high geothermal gradient that supports a number of commercial geothermal electricity generating plants. The heat from the geothermal field is the result of a shallow magma body from one or more spreading centers. The Salton Sea occupies the lowest part of the Salton Trough in Imperial County, CA.

Mud pots, mud volcanoes, and other structures formed by fluidized sediment are well known in geothermal regions.² They are often driven by rising CO₂ that entrains subsurface water and carries it to the surface. If the mud is low viscosity, mud pots form. If viscous, mud volcanoes form. They can change from one to the other as conditions vary, and may be hot (up to 100°C) or at ambient temperature.

Most endure for decades or more and undergo changes as meteoric water, underground plumbing, and flux of CO₂ change.

Salton Trough geothermal activity has been documented from a number of areas near Niland in Imperial County. These include:

1. Boiling mud pots and fumaroles in five fields near Mullet Island^{3,4}

2. The Davis–Schrimpf mud volcano field located at the intersection of Davis and Schrimpf Roads⁵⁻⁷
3. Ambient temperature mound springs near the intersection of Gillespie Road and State Route 111^{7,8}
4. Linearly aligned mud pots defining the Wister Fault (southeastern extension of the San Andreas Fault)⁹
5. Dry moderate-temperature (36°C) thermal vents on Red Island¹⁰

In this paper we describe the visual, physical and some chemical properties of a new, short-lived mud pot near Niland, Imperial County, CA (Figure 1).

Properties, appearance and time changes

Witnessing the formation and demise of a mud pot or mud spring is a rare occurrence. Such an event that took place on the Wister Fault⁹ starting in May 2018 (Figure 2). The mud pot was located at the edge of an agricultural field near the corner of English and Noffsinger roads. It was visited ten times between 12 June and 17 Jan 2019.

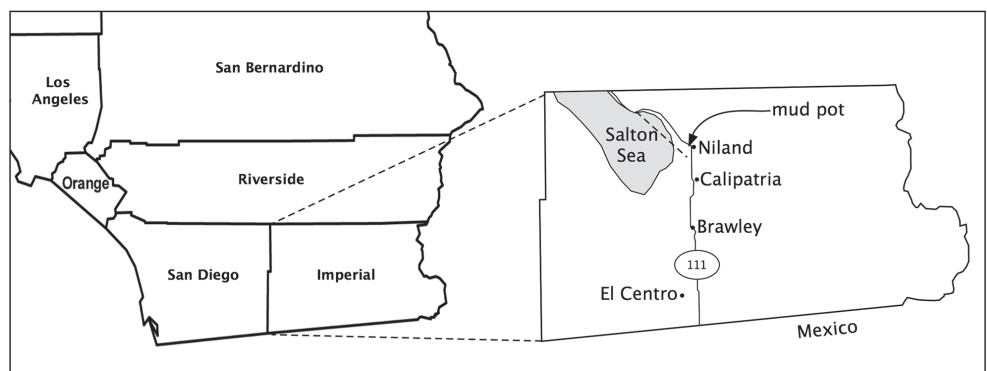


Figure 1. Map of mud pot locality near Niland, Imperial County, CA. Mud pot is located 1.6 km west of CA SR111 in Niland and just south of Noffsinger Rd. The approximate location of the Wister Fault is shown as a dashed line in the right-hand panel above.



Figure 2. Carol Zamora watching the mud pot in June 12, 2018. View looking north.

destroyed the beautiful mud pot, it did reveal some of its internal structure. Samples from the mud pot at various depths were collected at that time.

The mud pot (mud spring) initially eroded the surrounding sediments. The pot took the form of a small pond in a slightly depressed basin filled with muddy water a meter or so in diameter. The central region was vigorously bubbling and muddy water was being projected above the surrounding pond. Bubbling water emerging from the center of the basin was at 53°C (127°F), and remained at that temperature until late October, by which time the temperature had dropped to 47°C (117°F). To prevent spillage into the field, the farmer dug

Owing to the rapid changes on time scales of days-to-weeks, we cannot say what took place between visits. By November 22, 2018 the spring had ceased flowing. At that time, we observed that the mud pot had been cut in half by a newly dug irrigation trench. While the trench

a shallow trench leading south along an unnamed road and piled the dirt on the east side of the trench. No water was collected or analyzed.

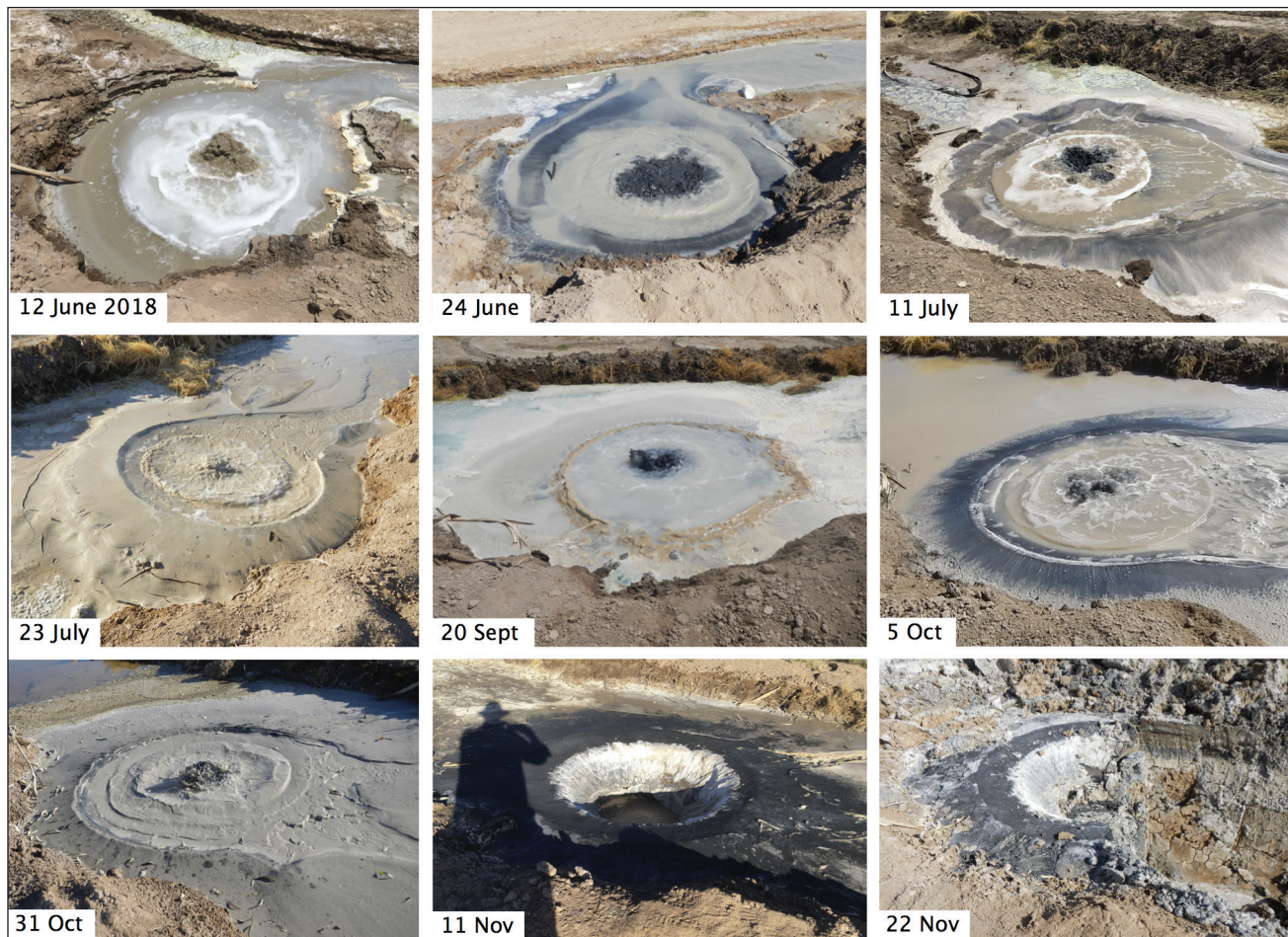


Figure 3. Time sequence showing the mud pot's changes between June 12 and 22 November 2018.

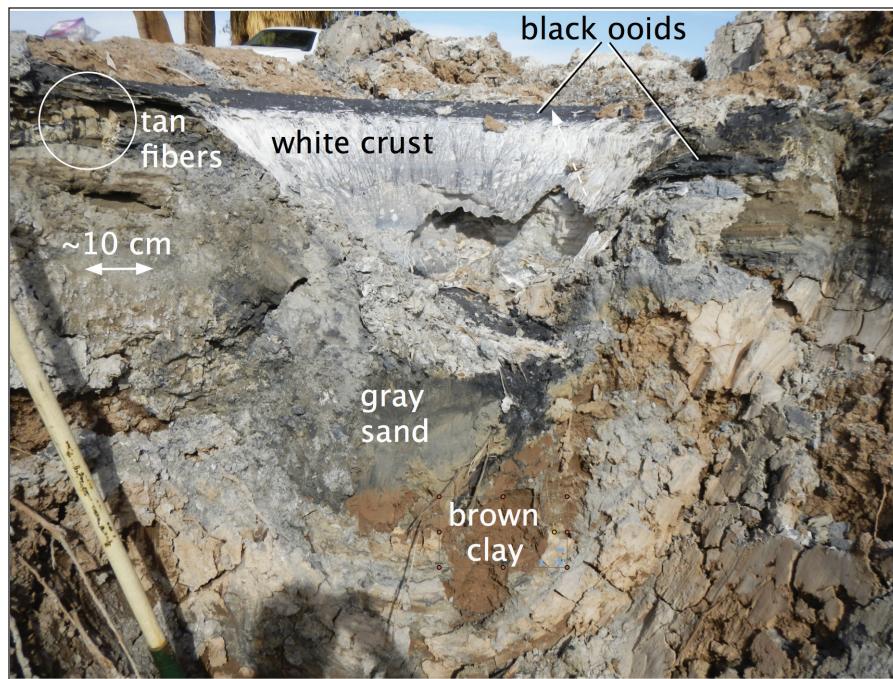


Figure 4. Cross-section view of inactive excavated mud pot on November 22, 2018. Tan fibrous material (circles), adjacent to a layer of black ooids, is located on both sides of the vent, just beneath the surface crust. The distribution of materials is not as orderly as we might have expected.

Following the initial observations described above, the pot was different with every visit, sometimes drastically so (Figure 3). In only 12 days after June 12, the emerging water changed from brown to black. The July 11 observations revealed a dark colored and slightly elevated rim of material surrounding the vent and above it, but only 12 days later (23 July), the vent rim was light brown, like the color of the emergent water. On September 20 the rim had vanished but a thin ring of fibrous, spongy material was seen, even as the emerging water had become black again. After September 20, the upwelling water remained black until the pot's demise, and the gray or black crater rim formed again, also being present to the end.

By November 11, the mud pot had changed significantly. Water was no longer emerging from it but the remaining black water was weakly bubbling approximately 0.25 meter below the crater rim. The



Figure 5. Hand sample of the white crust showing its rippled, corrugated surface. Water flow by gravity is from upper right to lower left along the obvious ripples.

inner cone was nearly white and contrasted sharply with the greatly enhanced, black material that surrounded it. Upon returning on November 22, we found that a 2 m-deep diversion channel had been excavated that bisected the mud pot and created a near vertical cross section (Figure 4) which allowed access to the mud pot's interior. The cross section of the pot was complicated, and we could not easily distinguish intrinsic complexity from mixing and distortion caused by the trenching device.

The remnant of the mud pot consisted of a conical depression, lined with a thin white crust (Figure 5) with a rippled surface, resembling white plastic balls that had partially melted together. It showed a fabric whose orientation was ~vertical, i.e., radial with respect to the pot's vertical axis. The white layer was about 0.25 m thick and was surrounded by

a slightly elevated apron of the same material coated with a thin layer (1-2 mm) of shiny rounded black ooids (Figure 6). Just beneath the surface, there are regions of fragile, low-density tan fibrous material adjacent to a layer of black ooids (Figure 7). The lower part of the vent is

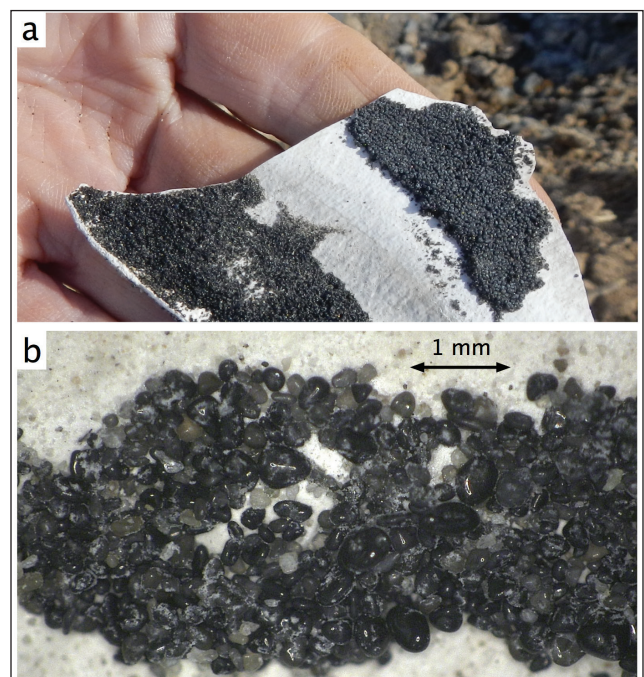


Figure 6. (a) Hand sample of the black layer on the white crust. (b) Optical micrograph of the black layer of ooids.



Figure 7. Tan fibrous material. The material was found on both sides of the vent, at about the same depth, ~10 cm below the surface. The strands were tightly packed and nominally vertically oriented. Locally, however, the fibers were curved. See Figure 4 for location. Photo taken 22 Nov 2018.

composed of gray sand and red-brown clay (bottom). The vent materials are set into muddy sand.

Laboratory Analyses

Selected samples were potted and vacuum impregnated with epoxy and cross-sectioned. These included a piece of the white horizontal crust covered with black ooids, the loosely cemented black ooids adjacent to the subsurface fibrous region, and a portion of the brown fibrous material. The potted samples were ground successively with 180-, 320- and 600-grit SiC paper and polished with 1-micron diamond paste. The samples were carbon coated and examined with a scanning electron microscope (SEM) equipped with a Si drift detector (SDD) energy dispersive spectrometer (EDS). Several samples were analyzed by

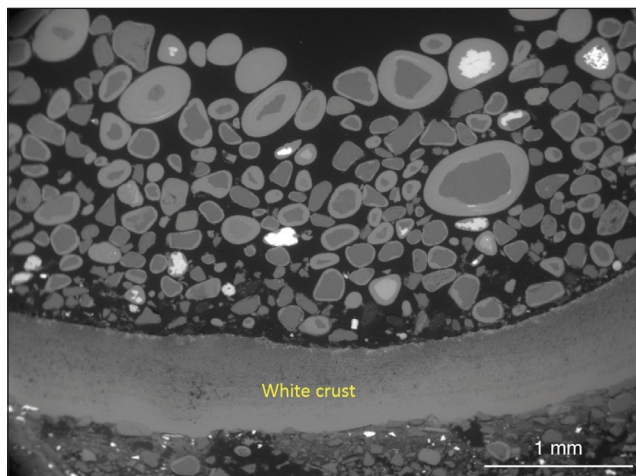


Figure 8. Backscattered SEM image of polished section through black ooids and underlying white crust. Bright nucleus at upper right consists of iron sulfide, other darker nuclei are silicates, primarily quartz and feldspars

X-ray diffraction (XRD) in order to identify the major phases present.

Black Ooids

The XRD pattern revealed that the surface of the black ooids was composed primarily of aragonite, the low temperature form of calcium carbonate. In contrast, the XRD pattern of the ground ooids consisted of major aragonite, quartz, and plagioclase feldspar (minor). Figure 8 shows a backscattered electron image of a cross section through the white crust and surficial black ooids. The thickness of the white crust varied between ~550-650 μm and EDS indicates it consists of Ca-C-O which is consistent with the identification as aragonite by XRD.

The ooids consist of layered aragonite of varying thickness that surround nuclei.

The ooids varied from equant to ellipsoidal in cross section with the maximum dimension ranging from 5 μm to 750 μm with a mean of 180 μm . The nuclei of the grains are primarily silicates (quartz, plagioclase and K-feldspar) but isolated grains of iron sulfide (pyrite) and barium sulfate (barite) were also observed. The latter appeared bright in the backscattered SEM images. From EDS, the overcoat of the ooids consists primarily of Ca-C-O, which is consistent with the identification of aragonite by XRD. The thickness ranges from 5-135 μm with an average of 30 μm . Some of the thicker rims contain localized discontinuous bands of iron sulfide (Figures 9, 10). While

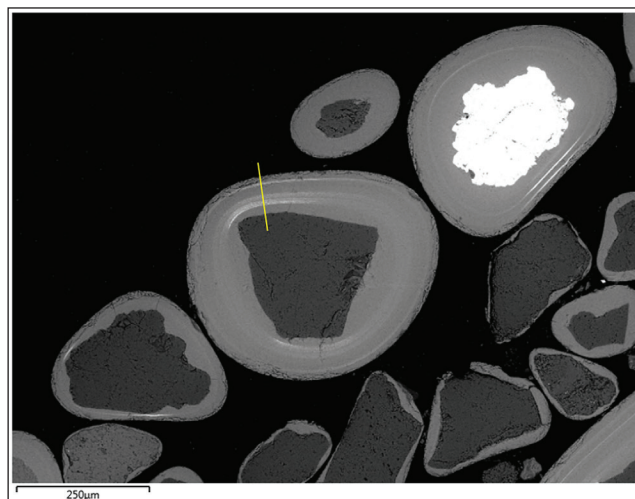


Figure 9. Backscattered SEM image of polished section through black ooids. Bright nucleus at upper right consists of iron sulfide, other darker nuclei are silicates. Notice partially periodic bands of light-colored iron sulfide around the two of the largest ooids. The line is the trace of the EDS line profile in Figure 9.

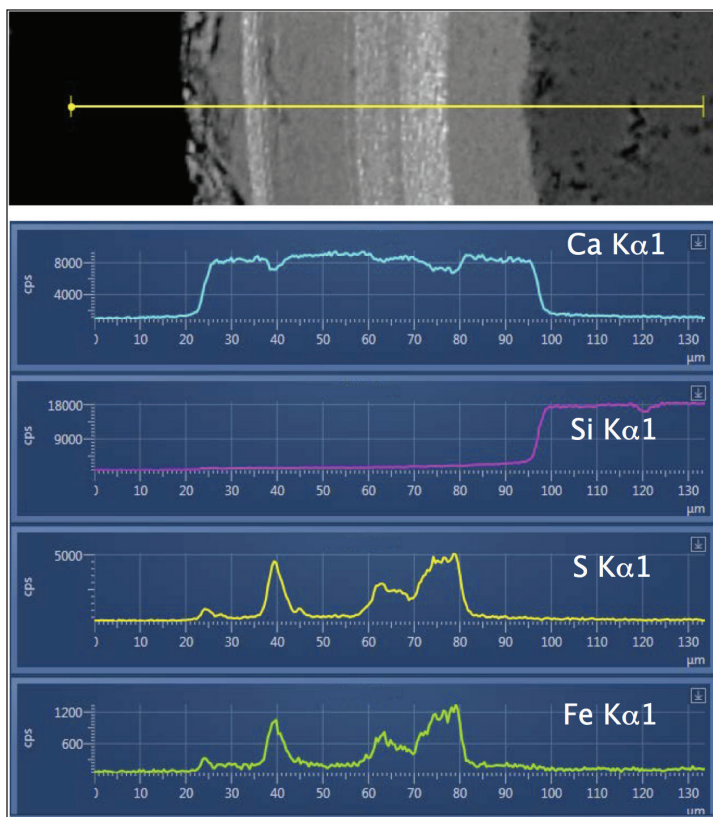


Figure 10. Top: Backscattered SEM image of cross section through the aragonite coating on a black ooid with a quartz nucleus in Figure 9. Bottom: EDS line profiles showing discontinuous bands of iron sulfide.

the color of pyrite in macro specimens is golden, the streak, which consists of fine particulates, is greenish black to brownish black. The size of the individual Fe-S grains in the rims is on the order of $< 5 \mu\text{m}$ and this probably accounts for the black appearance of the ooids. In the cross sections, not all beads displayed Fe-sulfides but, because of their localized discontinuous nature, the section does not always intersect them. A polished cross section through the poorly cemented subsurface layer of black ooids was very similar to the thin coating of black ooids on the surface of the white crust. The size of the ooids ranged from $30 \mu\text{m}$ to $375 \mu\text{m}$ with a mean of $150 \mu\text{m}$, which is slightly less than the ooids on the surface of the white crust ($180 \mu\text{m}$). The thickness of the overcoat varied from $5 \mu\text{m}$ to $50 \mu\text{m}$ with a mean of $15 \mu\text{m}$, which is half of that from the surface black ooids.

White Crust

The rippled surface of the white crust (Figure 5) is reminiscent of textured ridged surfaces of travertine in hot springs and caves. It was therefore no surprise to find that the XRD pattern of the surface of the white crust consisted predominantly of a mixture of aragonite, thenardite and quartz with minor halite, dolomite and perhaps barite. The presence of thenardite and halite was corroborated by SEM-EDS measurements

that showed thin discontinuous coatings on the black ooids that contained Na-S-O and Na-Cl, respectively.

Fibrous Material

The tan fiber bundles (Figure 7) are composed primarily of aragonite with minor amounts of quartz, based on the XRD pattern. They appear to be identical to “veinlets” in calcite, gypsum and other asbestiform minerals.^{11,12} Such growth requires specialized and rare conditions. According to Taber,¹¹

“Calcite and gypsum are not normally fibrous, and wherever they have developed this structure it is due to the physical conditions which have prevented crystal growth, except in one direction. Merrill has described fibrous incrustations of gypsum forming on the walls of caves [Figure 11], and notes that the growing crystals not infrequently force off pieces of the limestone of considerable size. Laboratory experiments and field investigations indicate that the essential conditions for the growth of fibrous minerals, such as calcite and gypsum, are: (i) the growing crystals must be in contact at their base with a supersaturated solution; and (2) the solution must be supplied through closely spaced capillary or subcapillary openings in the surface of the wall rock.”

The fibers in these veins are nominally solid single-crystals and may either grow from the walls of the veins (antiaxial) or from the center (syntaxial)¹³. Figure 12a shows an SEM image of a polished cross section through the tan fibrous aragonite vein. Surprising, the fibers are not solid single-crystals but consist of bundles of much smaller crystallites (Figure 12b). This is consistent with the fragile low-density nature of the material. The boundary between the two fibrous regions consists of calcium carbonate with varying degrees of porosity. Figures 12c and 12d show high magnification SEM images of the surface of one of the “fibers”. It consists of

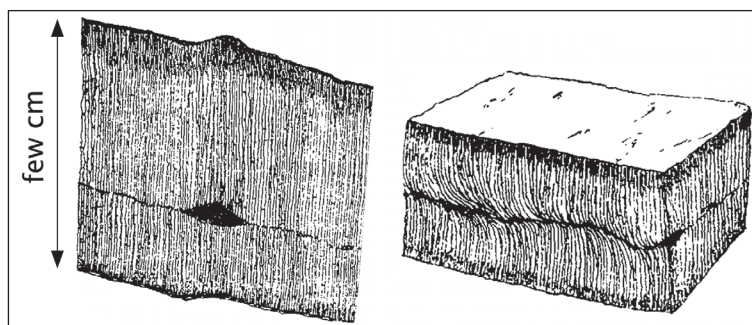


Figure 11. Veinlet structure of fibrous calcite, gypsum and asbestiform minerals. Adapted from Merrill¹².

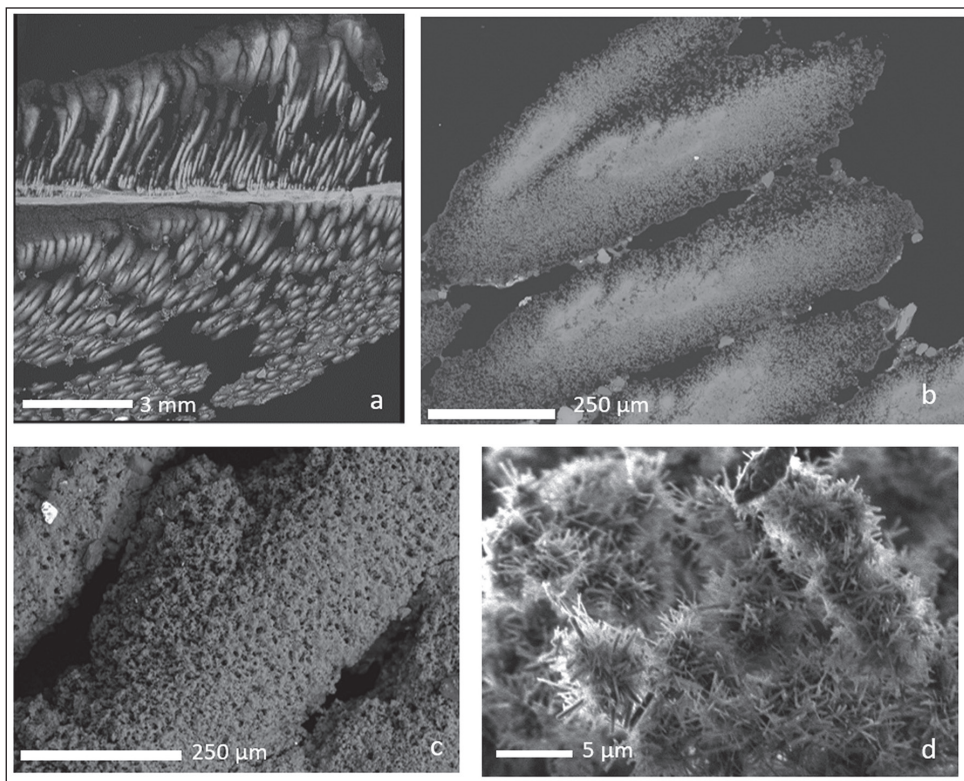


Figure 12. SEM images of the fibrous material. (a,b) polished cross sections. Notice porous nature of individual fiber bundles in (b). (c,d) surfaces of fibers consist of nano aragonite needles.

aggregates of minute ($0.1 \times 1.0 \mu\text{m}$) aragonite needles. As a result, the aragonite appears to represent a replacement (pseudomorph) of a preexisting fibrous mineral. The most likely candidates are calcite and gypsum. The fact that there is minimal sulfur in the system suggests that gypsum is unlikely, but it is difficult to explain the highly porous nature of the pseudomorphs if they represent replacement of calcite fibers. Replacement of aragonite by calcite is much more common than the reverse since calcite is the more thermodynamically stable. In contrast, pseudomorphs of aragonite after gypsum have been reported as a result of bacterial sulfate reduction under anaerobic conditions¹⁴ and pseudomorphs of calcite and aragonite after gypsum have been observed.¹⁵

Discussion

The new mud pot is the eastern-most in the Niland area showing elevated temperatures (53°C). It is one of a sequence of mud pots along the Wister Fault, the majority of which are inactive at this time, the exception being the reactivated mound spring at Gillespie Road and SR 111.⁸ Whatever was responsible for reactivation of this spring may also have influenced the formation of the new mud pot described here. Temperatures of other fumaroles, located to the west of the new mud pot, range from 100°C in the Mullet Island fumaroles,³⁻⁴ 62°C in the Davis-Schrimpf mud volcanoes,⁵⁻⁶ and 36°C in the Red Island vents.¹⁰

The black ooids are completely mantled with a tangentially-layered structure as shown by the repetitive banding of iron sulfides, when present. Their formation is probably analogous or related to that of cave pearls. CaCO_3 in some form is precipitated around a nucleus as a result of continuously agitated water saturated in calcium carbonate¹⁶. In the case of cave pearls, the agitation is a result of water dripping from the roof of the cave into splash cups,^{16,17} while with the mud pot, rising gas bubbles of carbon dioxide produced continuous or intermittent movement of sand grains. The incorporation of microscopic iron sulfide grains in discontinuous layers in many grains imparts the black color

to the ooids. While bulk iron sulfides (pyrite, marcasite) are brass-colored, it is noted that their streak (consisting of fine powder particles) are greenish to brownish black. Sulfides and sulfates are relatively common in hydrothermal solutions associated with magma bodies.¹⁻⁷ This can be related to the deep-seated magmatic nature of the geothermal fields in the Salton Trough.

It is easy to understand the formation of the black ooids on the surface where there can easily be free movement. The presence of a subsurface layer of black ooids also implies some movement of grains within the layer. This layer is adjacent to the fibrous aragonite and both are symmetrically disposed around the vent. Fibrous mineral veins generally form as a result of dilation of the vein during fiber growth—satin spar gypsum is an example.¹⁸

The white crust appeared late in the mud pot's life and after the water level had dropped below grade. It seems reasonable to suppose that the crust and ooids were produced and deposited by a supersaturated solution of CaCO_3 , and halite as the water level receded. Such deposition may be similar to the formation of travertine flowstone and other speleothems in caves.

The short ~ 7 -month life of the mud pot may be due to exhausting a pressurized subsurface CO_2 chamber. For some reason (earthquake?) an opening to the surfaced occurred, allowing CO_2 to migrate upward through the water table and drag water to the surface to form the mud pot. After depressurizing the CO_2 chamber, the mud pot

activity ceased. Transient or short-lived pressure releases have been previously observed in the area before.⁸

Based on many previous studies of fibrous minerals,^{11,12} we assume that the individual tan fibers (Figure 7, 11, 12) originally formed as single-crystals, probably of calcite or gypsum. The fact that they are now composed of porous aragonite and show no evidence of single, coherent crystals strongly suggests that they are pseudomorphs of aragonite after calcite or gypsum.

Conclusion

A new, small mud pot (mud spring) has been followed throughout its short, seven-month life. When serendipitously cross-sectioned, it revealed a number of interesting mineralogical phenomena of aqueous origin. The three main structures described here – white crust, black ooids and fibrous material are most easily explained in terms of processes commonly found in caves. It may be useful for understanding mud pots to view them in terms of cave systems and mechanisms.

Acknowledgements

We would like to thank Carol Zamora for introducing us to this mud pot and David M. Miller for many helpful comments on the manuscript.

References

1. <http://fire.biol.wvu.edu/trent/alles/GeologySaltonTrough.pdf>
2. <https://en.wikipedia.org/wiki/Mudpot>
3. Lynch, D.K., Hudnut, K.W., Adams, P.M., **Development and growth of recently-exposed fumarole fields near Mullet Island, Imperial County, California.** *Geomorphology* 195, 27-44 (2013). <http://doi.org/10.1016/j.geomorph.2013.04.022>.
4. Adams, Paul M., David K. Lynch, Kerry N. Buckland, Patrick D. Johnson and David M. Tratt, **Fumarole Sulfate Mineralogy Related to Geothermal Fields at the Salton Sea, Imperial County, California,** *Journal of Volcanology and Geothermal Research*, 347 (Nov) 15-43 (2017).
5. Mazzini, A., Svensen, H., Etiope, G., Onderdonk, N., Banks, D., **Fluid origin, gas fluxes and plumbing system in the sediment-hosted Salton Sea geothermal system (California, USA).** *J. Volcano. Geotherm. Res.* 205 (3-4), 67-83 (2011). <http://doi.org/10.1016/j.jvolgeores.2011.05.008>.
6. Onderdonk, N., Shafer, L., Mazzini, A., Svensen, H., **Controls on the expression and evolution of gryphons, mud pots, and caldera features at hydrothermal seeps in the Salton Sea Geothermal Field, Southern California.** *Geomorphology* 130 (3-4), 327-342 (2011). <http://doi.org/10.1016/j.geomorph.2011.04.014>.
7. Adams, P.M., Lynch, D.K., **A mineralogical inventory of geothermal features southeast of the Salton Sea, Imperial County, California.** 2014 Desert Symposium Field Guide and Proceedings (R. Reynolds, ed.), Cal. State Univ. Fullerton Desert Studies Consortium, 100-111 (2014). <http://nsm.fullerton.edu/dsc/images/DSCdocs/2014Notadroplefttodrink.pdf#page=100>.
8. Lynch, D. K., R. Travis Deane and Justin D. Rogers, **A Mysterious Moving Mud Pot near Niland CA.,** (2019, this volume)
9. Lynch, D.K., Hudnut, K.W., **The Wister mud pot lineament: Southeastward extension or abandoned strand of the San Andreas Fault?** *Bull. Seismol. Soc. Amer.* 98 (4), 1720-1729 (2008). <http://doi.org/10.1785/0120070252>.
10. Lynch, D.K., Adams, P.M., **Hot volcanic vents on Red Island, Imperial County, California.** 2014 Desert Symposium Field Guide and Proceedings (R. Reynolds, ed.), Cal. State Univ. Fullerton Desert Studies Consortium, 117-120 (2014). <http://nsm.fullerton.edu/dsc/images/DSCdocs/2014Notadroplefttodrink.pdf#page=117>.
11. Taber, Stephen, **The Origin of Veinlets in the Silurian and Devonian Strata of Central New York,** *The Journal of Geology*, 26(1) (Jan. - Feb.), 56-73 (1918). <https://www.jstor.org/stable/30078162>
12. Merrill, G. P., **On the Formation of Stalactites and Gypsum Incrustations in Caves,** *Proc. U.S. Nat. Mus.*, XVII, 81 (1894).
13. Bons, P. D. and Montenari, M., **The formation of antiaxial calcite veins with well-developed fibres, Oppaminda Creek, South Australia,** *Journal of Structural Geology*, 231-248 (2005).
14. Anadon, P., L. Rosell and M.R. Talbot, **Carbonate replacement of lacustrine gypsum deposits in two Neogene continental basins, eastern Spain,** *Sedimentary Geology*, 78 201-216 (1992).
15. Fernández-díaz, L., Pina, C. M., Astilleros, J. M. and Sánchez-Pastor, N., **The carbonatation of gypsum: Pathways and pseudomorph formation,** *American Mineralogist*, 94, 1223-1234 (2009).
16. Davies, Peter J., B. Bubela and James Ferguson, **The formation of ooids,** *Sedimentology*, 25, 703-730 (1978)
17. Donahue, Jack, **Genesis of oolite and pisolith grains: An energy index,** *J. Sedimentary Petrology*, 39(4) 1399-1411 (1969).
18. <https://www.mindat.org/min-8574.html>